FROM THE PERIODIC NEAR FIELD TO THE THREE-DIMENSIONAL TURBULENT MOTIONS IN THE FAR FIELD OF A CYLINDER WAKE

Gregory A. Kopp
Boundary Layer Wind Tunnel Laboratory
University of Western Ontario, London, Ontario, N6A 5B9, Canada

Anton Vernet
Departament d'Enginyeria Mecànica
Campus Sesclades, ETSEQ,
Universitat Rovira i Virgili, Tarragona, Catalunya, Spain

Francesc Giralt
Departament d'Enginyeria Química
Campus Sesclades, ETSEQ,
Universitat Rovira i Virgili, Tarragona, Catalunya, Spain

ABSTRACT

The typical coherent structure in the far wake region of a circular cylinder is known to be shaped like a horseshoe with jet-like motions in its centreplane. Strong evidence is given that similar motions exist in both the near and intermediate wakes. Pattern recognition analysis of multi-probe hot-wire data indicate that vortices aligned further than average from the wake centreline exhibit the jet-like features characteristic of the far wake structures. In fact, analysis of hot-wire signals near the edge of the wake just 2 diameters downstream of the cylinder indicate that the "footprint" of the jet-like motions exists early in the formation of the vortex street.

INTRODUCTION

There is now much evidence that the wake structures far downstream of a circular cylinder are shaped like horseshoes (Mumford, 1983; Ferre & Giralt, 1989ab; Giralt & Ferre, 1993; Kopp et al., 1995; Vernet et al., 1999). In the centreplane of these structures the motions are very much like Grant's (1955) and Townsend's (1956) "mixing jets". Kopp et al. (2002) recently showed that these motions are responsible for engulfment and the growth of the wake, and that this process has a suprisingly long time scale, consistent with the observed "frozen" behaviour of far wakes. In fact, they found that the entrainment time scale relative to the local wake time scale (the mean velocity half width over the maximum velocity defect) is on the order of 10. Examining ensemble averages of these entrainment vortices, they concluded that the eddy time scale was also about one order of magnitude larger that the local time scale, so defined.

The concept of self-preservation implies that the large, energy containing eddies should be in equilibrium with the flow. Since wakes are (at least approximately) self-preserving by about x/d ~ 100, the turbulent structures are in (at least approximate) equilibrium with the flow by this location. The Karman vortices are normally visible until around x/d ~ 50, although they are significantly randomized much earlier in the flow. Since the time scales at self-preservation indicate long lasting structures, one would expect to see some structural similarity with the location where the Karman vortices are gone. This has not been investigated previously although Browne et al. (1989) have shown, using spectral analysis, that a peak that is visible in in v-autospectra or in u-v coherence functions the far wake region is also discernible in the near wake (although with much less energy than the Kármán vortices).

There has been debate in the literature about the effect of initial conditions on the structures observed in far wakes, but many questions yet remain. For example, Keffer (1965) postulated that hairpin vortices could form right at the cylinder. Hussain and Hayakawa (1987) provided evidence that the far wake structures are the result of bending of the Kármán vortices by the secondary 'rib' structures. Cimbala et al. (1988) have given strong evidence that it is the

instability of the mean velocity profile, which is the source of the far wake structure (which they called the 'secondary vortex street'). Interestingly, Wygnanski et al. (1986) speculated that the perturbation required for the instability was the coherent structure itself. Our time-scales in the self-preserving region are consistent with this.

The objective of the current work is to make a clearer connection between the far wake structures with those in the near wake. Particular emphasis is placed on the dynamically important jet-like motions.

EXPERIMENTAL DETAILS

Figure 1 shows the experimental set up. A circular cylinder was placed in a uniform freestream with U_o = 9.0 m/s so that the Reynolds number, based on the cylinder diameter, d = 11.6 mm, was Re = 6700. A rake of eight X-wire probes were located at downstream positions x/d = 16, 30, 60 and 90, with a probe spacing of $\Delta z = \Delta y$ =7 mm = 0.60d. The rake was placed vertically measuring the streamwise (u) and lateral (v) components of the velocity.

Time is normalised using Taylor's hypothesis and the cylinder diameter, $x^*=-U_o\Delta t/d$. The signals were low pass filtered at 2000 Hz and then digitally sampled at a rate of 5000 samples per second per channel for 40 seconds. In addition, some single X-wire data was taken closer to the cylinder in regions where the turbulence intensity and direction of flow are such that reliable time series measurements were possible (Kawall et al., 1983).

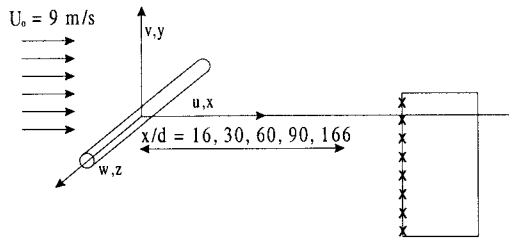

Figure 1. A sketch of the experimental set-up. Probe 1 is uppermost.

A convection velocity, U_c, has been subtracted from the streamwise component in the analysis presented below. The convection velocity has been determined via trial-and-error so that the velocity field has a pattern that coincides with the centre of spanwise vorticity contours when a focus is identified. In the horizontal plane only fluctuations of the velocity vector have been used. The convection velocity for each streamwise location is given in Vernet et al. (2002).

IDENTIFICATION OF CRITICAL POINTS

Critical points are defined as locations where the velocity is zero so that the streamline slope is indeterminate (Perry and Chong, 1987). Various patterns are allowed around critical points based on the series expansion of the velocity field around the critical point. Difficulties in detecting critical points arise when coarsely spaced experimental data, such as that obtained by multiple X-wire probes, are used since the velocity gradient tensor is incomplete or poorly resolved. It is poorly resolved because data obtained by rakes of hot-wires are inherently coarse when compared to the size of the region where the series expansion around the critical point is valid. The 'noisy background' of turbulence in which the critical points are embedded adds difficulty since it causes deviation in the measured critical point patterns from the idealised patterns.

Since identification of critical points in coarsely spaced experimental data is uncertain, it seems natural to develop a pattern recognition technique to identify these motions based on fuzzy logic. Fuzzy logic was originally developed by Zadeh (1965) as a new method to deal with uncertainty. It allows a quantification of the uncertainty so that decisions can be made. In traditional logic, something is either certain or uncertain; a proposition is either true or false. In contrast, common experience tells us that many things are partly true and partly false at the same time. Fuzzy logic is the mathematical formalism to handle these situations.

Clustering is a technique used to partition data sets, where each cluster has similar features. The central value of the cluster in the pattern space is the cluster centroid, or simply centroid. Grouping of the data is generally done by applying some kind of similarity function over the data set. This function (called the membership function) gives a value, μ_{ij}, of the membership of the *ith* individual element in the *jth* cluster. A full description of the fuzzy clustering technique to detect and classify critical points can be found in Vernet & Kopp (2002), although the main points of the technique are given below.

By direct observation (see Vernet & Kopp, 2002) of the experimental data it was determined that the patterns around the critical points have a spatial extent of about seven points in the streamwise co-ordinate and three sensors in the current set-up. Each of the patterns is represented by a feature vector, $X_i=\{\alpha_1, \alpha_2 \ldots \alpha_{20}\}$, where the elements of X are the angles calculated from the two velocity components, as suggested by Ferre-Gine et al. (1997). This procedure means losing the magnitude of the velocity vectors in the classification procedure. However, it is the curvature of the streamlines, which is most important, and this is most easily dealt with via the phase information. The clustering procedure uses the fuzzy C-means (FCM) algorithm. This algorithm is based on the minimisation of the objective function, J_m,

$$J_m = \sum_{i=1}^{c}\sum_{j=1}^{n}(\mu_{ij})^m \left\| X_j, V_i \right\|^2$$

where

$$V_i = \frac{\sum_{j=1}^{n}(\mu_{ij})^m X_j}{\sum_{j=1}^{n}(\mu_{ij})^m}$$

c is the number of clusters, n is the number of feature vectors, μ_{ij} is the membership of vector i in cluster j, X is the feature vector, V is the centroid (i.e., the vector that defines the centre of the cluster, $\|\cdot\|$ is the Euclidean distance and m

is the fuzzy partition exponent. A larger m indicates a fuzzier partition, while for $m = 1$ the partition is hard. Membership measures the grade each feature vector belongs to one cluster and varies between 0 and 1. The objective function, J_m, is a measure of the differences between the data analysed and the centroids weighted by $(\mu_{ij})^m$. Each feature vector belongs to all the clusters of the partition in some sense and, therefore, has a value for each cluster. The membership is calculated from

$$\mu_{ij} = \frac{\left(1/\left\|X_j, V_i\right\|\right)^{1/(m-1)}}{\sum_{i=1}^{c}\left(1/\left\|X_j, V_i\right\|\right)^{1/(m-1)}}$$

In addition,

$$\sum_{i=1}^{c}\mu_{ij} = 1$$

for i = 1,2,3...c, j = 1,2,3...n

The process is iterative with the following steps: (a) initialize μ_{ij} using a random function, (b) calculate the centroids, (c) update μ_{ij} and (d) calculate J_m. The steps (b) – (d) are repeated until the difference between two consecutive J_m is less than a fixed threshold. This generates a membership matrix which is used to partition the data set. Each feature vector is classified in the cluster for which it has the highest membership value. The fuzzy partition exponent (m) and the number of clusters (c) are selected using,

$$S = \frac{\sum_{i=1}^{c}\sum_{k=1}^{n}\mu_{ik}^2\left\|x_k - v_i\right\|^2}{n\left(\min_{i\neq j}\left(\left\|v_i - v_j\right\|^2\right)\right)}$$

The numerator measures the "compactness" of the clusters. The smaller this value is, the more compact the clusters in the partition are. The denominator measures how well separated the clusters are with a larger value indicating better separation. Globally, a smaller S indicates a partition in which clusters are compact and well separated from each other. The minimum S provides the optimum c and m values to partition the data set.

Once the data are classified into the different clusters, a simple ensemble average of the events in each cluster is performed to obtain the prototypical event that characterizes each cluster. Further details can be found in Vernet & Kopp (2002).

ANALYSIS

Karman Vortices in the Intermediate Wake

The fuzzy clustering algorithm was applied to the current wake data at all streamwise locations. For brevity, only the results at x/d = 16 will be presented. The clustering algorithm allowed for accurate alignment of similar classes of patterns. For example, Figure 2 depicts the ensemble average of a cluster of foci centred on the third probe (y* ~ -0.5). The patterns identified are only associated with the central focus, but a wider averaging window allows the periodicity in the flow (if it exists) to be observed. This pattern is very similar to those obtained by various phase averaging or eddy identification techniques, and is only shown to indicate that the behaviour of the present flow is what would be expected, and that the present pattern recognition technique is also working as expected. More details can be found in Vernet & Kopp (2002) and Vernet et al. (2002).

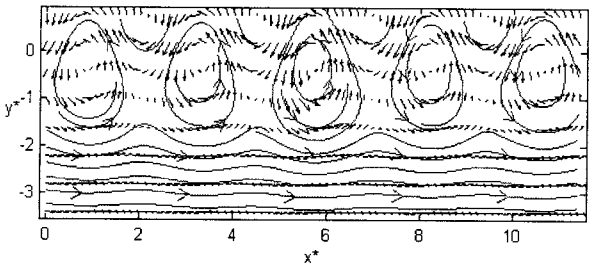

Figure 2. Ensemble-averaged foci centred on probe 3.

Jet-like Structures in the Intermediate Wake

Figure 3 shows the ensemble averages of the saddle points centred further from the centre of the wake than the average location of the saddle points. Figure 4 shows the same ensemble average with the local mean velocity removed. The ensemble average (centred at x* ~ 6, y* = -3) has lost the symmetry observed in Figure 2 with the outward lateral velocity fluctuations being significantly larger than the inward lateral velocities for the vortex centred between ~6 < x* < ~8. This pattern, which is stronger downstream (see Vernet et al., 2002), is typical of the far wake coherent structures which make up the turbulent bulges, in particular, the jet-like motions in the centreplane of the horseshoe structures (Vernet et al., 1999; Kopp et al., 2002). The ensemble-averaged velocity fluctuations in Figure 4 show these features more clearly.

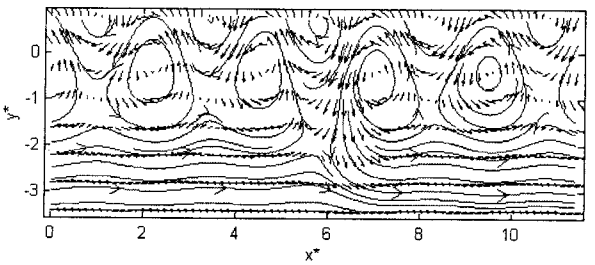

Figure 3. Ensemble-average of velocities classified as saddle points in the vertical plane at x* ~ 6 and y* ~ -3 for x/D = 16.

Continuous wavelet transforms of the u and v ensemble averages in Figure 4 for the probe at y* ~ -3 (the sixth probe from the top, in the plot) are depicted in Figure 5. For ~6 < x* < ~7, there is an observed increase in energy at larger scales (or smaller frequencies). Kiya and Matsumura (1988), in their analysis of the incoherent signals, found that the secondary rib structures have a significant fraction of their energy at frequencies smaller than the Strouhal frequency, and that this energy was concentrated in the saddle region.

Figure 5 shows that the jet-like motions are also associated with energy at lower frequencies. In this case, there is still a significant fraction of energy at the main shedding frequency, consistent with the pattern observed for the sixth sensor (y* ~ -3) in Figure 3; however, there is significantly increased energy at the lower frequencies. Continuous wavelet transforms of individual patterns used in the ensemble average indicate similar information, though with greater variability, as would expected. Note that Kiya and Matsumura removed the coherent motions from the signals prior to their analyses.

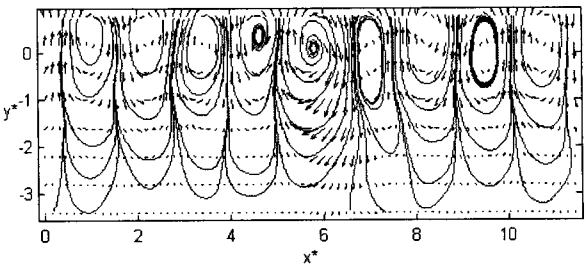

Figure 4. The same ensemble average as in Figure 2, but with the local mean (time averaged) velocity removed from each probe.

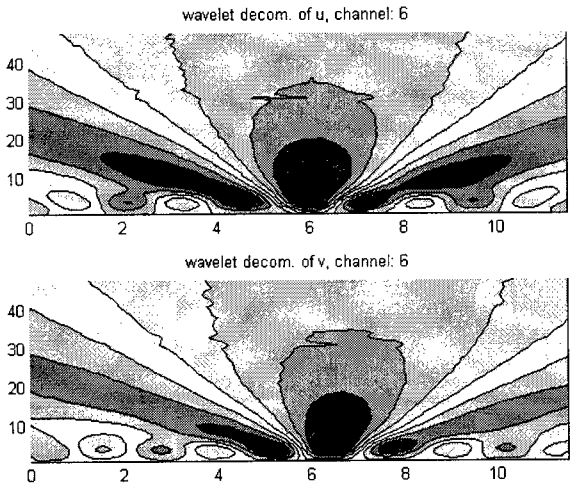

Figure 5. Continuous wavelet transform, using the Mexican Hat, of the ensemble average for probe 6 (y* ~ -3) depicted in Figure 4.

Three-Dimensional Structures in the Near Wake

The near wake region of circular cylinders exhibits complex flow patterns even at relatively low Reynolds numbers. The first instability leads to the Karman vortices. As the Reynolds number is increased, three-dimensional instabilities begin. Williamson (1996) provides a recent, comprehensive review for relatively low Reynolds number flows, while Chyu and Rockwell (1996) discuss the three-dimensional structures at higher Reynolds numbers. Our interest here is how far upstream, towards the formation region, can "jet-like" structures, with characteristics similar to those observed in the far wake, be observed. To do this a conditional averaging technique was utilized, along with the continuous wavelet transform and the single X-wire data taken at various locations in the near wake region.

The procedure is as follows. First, the probability density functions of the velocity fluctuations were obtained. Using this, a threshold was (arbitrarily) chosen for identifying the "jets". For example, at x/d = 16, a lateral fluctuation of –2 m/s was used. Second, since the jets are typically of 8-10 data points in duration (c.f., Figure 4), events with lateral velocity fluctuations of larger magnitude than the threshold for 6 points were accepted for averaging. Finally, the "events" were ensemble-averaged and a continuous wavelet transform of the ensemble average was taken using the Mexican Hat wavelet. Figure 6 depicts the resulting ensemble average at x/d = 16 and y/d = -2 for the new data while Figure 7 depicts the resulting wavelet transform. These show excellent agreement with the earlier data shown in Figures 4 and 5, although the current wavelet data is much smoother in appearance. This analysis was performed for data obtained from x/d = 2, 4, 6, 8, 10, 12 and 16 in the lower half wake near the outer edge where the turbulence intensities and instantaneous flow directions were such that instantaneous velocity data could be reliably measured with X-wires (Kawall et al., 1983).

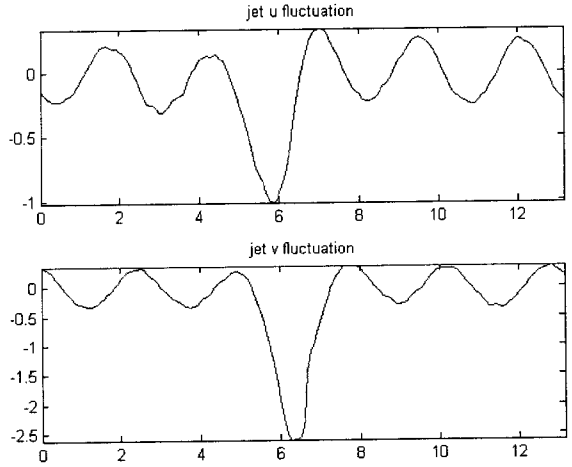

Figure 6. Ensemble average of the "jets" at x/d 16 and y/d = -2.

Pertaining to the wavelet transforms and plots, note that the wavelet scale (plotted on the vertical axis), a, for the Mexican Hat wavelet, is related to frequency, f, via

$$f = 0.251\, f_{sampling}/f$$

$f_{sampling}$ is the sampling frequency of the data (Hangan, 2003). Thus, for $f_{sampling}$ = 5000 and the Strouhal frequency of 160 Hz, a = 7.8, consistent with the observations in Figure 7. (In Figures 3 and 4, every other point was plotted so that the $f_{sampling}$ was 2500 and a ~ 4.)

Figures 8 and 9 depict the wavelet transform results for x/d = 8 and 2, respectively. It is interesting to observe that overall patterns are similar to those at x/d = 16, although some of the details are quite different. In particular, it is

clear that a larger and larger proportion of the energy is concentrated at the Strouhal frequency. Hussain and Hayakawa (1987), and others, point out that the ribs act to deform the Karman vortices, kinking them outwards. While we don't have spatial ensemble averages at this location, clearly, at x/d = 16, the footprints of the jets, as identified with the current approach, are associated with foci which are further from the centreline.

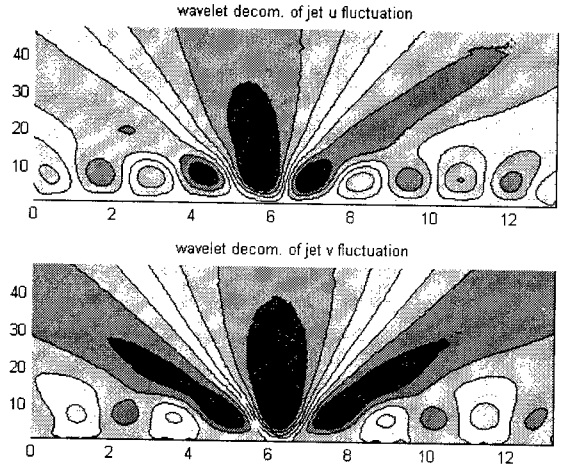

Figure 7. Continuous wavelet transforms of the ensemble averages in Figure 6.

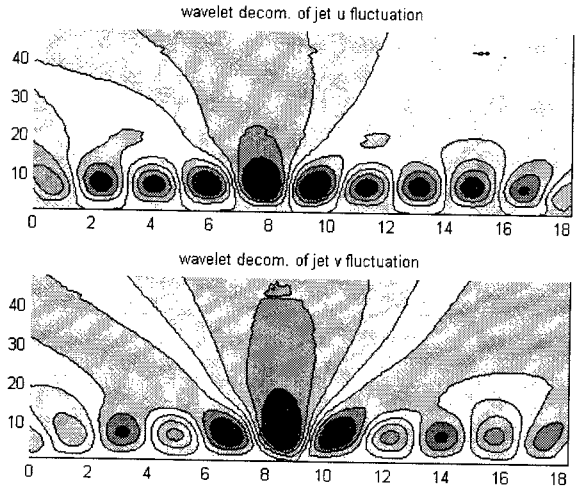

Figure 8. Continuous wavelet transforms of <u> and <v> at x/d = 8 and y/d = -1.5.

DISCUSSION

Using spectral analysis Browne et al. (1989) found a broadband spectral peak at a frequency slightly lower than the dominant Kármán frequency in the near wake. These authors concluded that this broadband peak was related to the origin of the far wake structures. Examination of the ensemble averaged velocity fluctuations in Figure 4 shows that the pattern associated with the jet-like motions is slightly larger than the patterns at the nominal vortex shedding wavelength. This is reflected by the distortion of the stream patterns, which implies a slightly larger wavelength for these motions and, therefore, a lower frequency. As the flow develops, the outward kinking of the main vortex structure would continue due to its increasing alignment with the mean strain field (which would act to enhance these structures through vortex stretching) and the decreasing action of the ribs (since the strain field in which they exist is growing weaker).

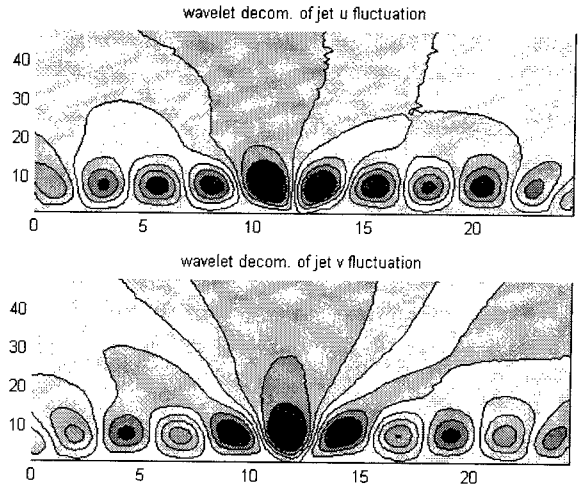

Figure 9. Continuous wavelet transforms of <u> and <v> at x/d = 2 and y/d = -1.5.

Data from other flows can also help to explain the role of the secondary rib structures in the present flow. For example, in the wake of a porous mesh strip, Kopp & Keffer (1996b) showed that the flow through the screen acted to reduce the strain field between adjacent Karman vortices. Although the Reynolds number of the flow was 5000, the flow field was highly regular and much more two-dimensional. Since the ribs were so weak, the Karman vortices could decay without much interference. Horseshoe vortices were observed in this flow in the far field, though the spanwise vorticity at the "top" was much lower yielding a rather different self-preserving state (Louchez et al., 1987; Kopp and Keffer, 1996a).

The oscillating circular cylinder of Kopp et al. (2003) also makes the main Karman vortices much more two-dimensional. In this case, however, the vortices are stronger than for a stationary cylinder, as are the resulting ribs. The cylinder oscillations appear to reduce the larger three-dimensional instabilites so that vortex dislocations are also reduced (accounting for the increased two-dimensionality of the Karman vortices). Although they only present near wake data, the wake is considerably thinner than the stationary cylinder wake, raising some questions over the precise role of the ribs. It would appear, although more analysis and experiments are clearly required, that the ribs need the initial displacement of the Karman vortices, perhaps caused by the dislocations, in order to act early in the wake.

CONCLUSIONS

The jet-like motions, key to the engulfment mechanism in the far wake, are observed in ensemble averages near the outer edges of the wake at x/d = 16. Wavelet transforms of ensemble averages indicate that "footprints" of these motions exist in the near wake as well, even at x/d = 2. This early formation allows the structures to come into equilibrium with the mean flow so that cylinder wakes are (approximately) self-preserving by x/d ~ 100. The jet-like motions appear to be related to the rib structures observed by many researchers. Since the far wake structures are three-dimensional, it is natural that three-dimensionalities in the formation of the Karman vortices play a key role in this development.

ACKNOWLEDGEMENTS

This work was financially supported by the DGICYT projects PB96-1011 and PPQ2000-1339(Spain), CIRIT project 1998SGR-00102 (Catalunya), NSERC (Canada), and a University of Western Ontario VP(R) Grant. A.Vernet was supported by the Universitat Rovira i Virgili during the portion of the work carried out in Canada. G.A. Kopp gratefully acknowledges the support of the Canada Research Chairs Program.

REFERENCES

Browne, L.W.B., Antonia, R.A., & Shah, D.A., 1989, "On the origin of the organised motion in the turbulent far-wake of a cylinder," *Exp. Fluids,* vol. 7, pp. 475-480.

Chyu, C. & Rockwell, D., 1996, "Evolution of patterns of streamwise vorticity in the turbulent near wake of circular cylinder," *J. Fluid Mech.*, vol. 320, pp. 117-137.

Cimbala, J.M., Nagib, H.M. & Roshko, A., 1988, "Large structure in the far wakes of two-dimensional bluff bodies," *J. Fluid Mech.,* vol. 190, pp. 265-298.

Ferré, J.A. & Giralt, F., 1989a, "Pattern recognition analysis of the velocity field in plane turbulent wakes," *J. Fluid Mech.,* vol. 198, pp. 27-64.

Ferré, J.A. & Giralt, F., 1989b, "Some topological features of the entrainment process in a heated turbulent wake," *J. Fluid Mech.,* vol. 198, pp. 65-77.

Ferré, J.A., Mumford, J.C., Savill, A.M. & Giralt, F., 1990, "Three-dimensional large-eddy motions and fine-scale activity in a plane turbulent wake," *J. Fluid Mech.,* vol. 210, pp. 371-414.

Ferre-Gine, J., Rallo, R., Arenas, A. & Giralt, F., 1997, "Extraction of structures from turbulent signals," *Art. Intell. Eng.*, vol. 11, pp. 413-419.

Giralt, F. & Ferré, J.A., 1993, "Structure and flow patterns in turbulent wakes," *Phys. Fluids A*, vol. 5, pp. 1783-1789.

Grant, H.L., 1958, "The large eddies of turbulent motion," *J. Fluid Mech.,* vol. 4, pp. 149-190.

Hangan, H., 2003, private communication.

Hussain, A.K.M.F. & Hayakawa, M., 1987, "Three-dimensionality of organised structures in a plane turbulent wake," *J. Fluid Mech.*, vol. 206, pp. 375-404.

Kawall, J.G., Shokr, M. & Keffer, J.F., 1983, "A digital technique for the simultaneous measurement of streamwise and lateral velocities in turbulent flows," *J. Fluid Mech.*, vol. 133, pp. 83-112.

Keffer, J.F., 1965, "The uniform distortion of a turbulent wake," *J. Fluid Mech.*, vol. 22, pp. 135-159.

Kiya, M. & Matsumura, M., 1988, "Incoherent turbulence structure in the near wake of a normal plate," *J. Fluid Mech.,* vol. 190, pp. 343-356.

Kopp, G.A., Fathi, S., Havel, B., Martinuzzi, R.J. & Galsworthy, J., 2003, "The velocity field in the near wake of a freely-oscillating circular cylinder at lock-in," *to be presented at the 3rd International Symposium on Turbulence and Shear Flow Phenomena*, Sendai, Japan, June 2003.

Kopp, G.A., Giralt, F., & Keffer, J.F., 2002, "Entrainment vortices and interfacial intermittent turbulent bulges in a plane turbulent wake," *J. Fluid Mech.*, vol. 469, pp. 49-70.

Kopp, G.A., Kawall, J.G. & Keffer, J.F., 1995, "The evolution of the coherent structures in a uniformly distorted plane turbulent wake," *J. Fluid Mech.*, vol. 291, pp. 299-322.

Kopp, G.A. & Keffer, J.F., 1996, "Coherent structures in two uniformly distorted plane turbulent wake," *Phys. Fluids*, vol. 8, pp. 2706-2711.

Kopp, G.A. & Keffer, J.F., 1996, "The near wake region of a high solidity mesh strip," *Phys. Fluids*, vol. 8, pp. 2712-2715.

Louchez, P.R., Kawall, J.G. & Keffer, J.F., 1987, "Investigation of the detailed spread characteristics of plane turbulent wakes," Turbulent Shear Flows 5 (ed. By Bradbury et al.), Springer, pp. 98-109.

Mumford, J.C., 1983, "The structure of the large eddies in fully developed turbulent shear flows. Part 2. The plane wake," *J. Fluid Mech.*, vol. 137, pp. 447-456.

Perry, A.E. & Chong, M.S., 1987, "A description of eddying motions and flow patterns using critical-point concepts," *Ann. Rev. Fluid Mech.*, vol. 19, pp. 125-155.

Townsend, A.A., 1956, The Structure of Turbulent Shear Flow, Cambridge University Press.

Vernet, A. & Kopp, G.A., 2002, "Classification of turbulent flow patterns with fuzzy clustering," *Eng. App. Art. Intell.*, vol. 15, pp. 315-326.

Vernet, A., Kopp, G.A., Ferre, J.A. & Giralt, F., 1999, "Three-dimensional structure and momentum transfer in a turbulent cylinder wake," *J. Fluid Mech.*, vol. 394, pp. 303-337.

Vernet, A., Kopp, G.A. & Giralt, F., 2002, "Critical points ant three-dimensional features in a plane turbulent wake," *Engineering Turbulence Modelling and Experiments - 5* (ed. Rodi, W. & Fueyo, N.), Elsevier, pp. 465-474.

Williamson, C.H.K., 1996, "Vortex dynamics in a cylinder wake," *Ann. Rev. Fluid Mech.*, vol. 28, pp. 477-539.

Wygnanski, I., Champagne, F. & Marasli, B., 1986, "On the large-scale structures in two-dimensional, small-deficit, turbulent wakes," *J. Fluid Mech.*, vol. 168, pp. 31-71.

Zadeh, L.A., 1965, "Fuzzy Sets," *Information and Control,* vol. 8, pp. 338-353.